Clay Nanopaper with Tough Cellulose Nanofiber Matrix for Fire Retardancy and Gas Barrier Functions

ARTICLE *in* BIOMACROMOLECULES · FEBRUARY 2011

Impact Factor: 5.75 · DOI: 10.1021/bm101296z · Source: PubMed

5 AUTHORS, INCLUDING:

Andong Liu
KTH Royal Institute of Technology
6 PUBLICATIONS **333** CITATIONS
SEE PROFILE

Lars Berglund
KTH Royal Institute of Technology
155 PUBLICATIONS **6,305** CITATIONS
SEE PROFILE

Biomacromolecules

ARTICLE

pubs.acs.org/Biomac

Clay Nanopaper with Tough Cellulose Nanofiber Matrix for Fire Retardancy and Gas Barrier Functions

Andong Liu,*[,†] Andreas Walther,[‡] Olli Ikkala,[‡] Lyuba Belova,[§] and Lars A. Berglund*[,†]

[†]Wallenberg Wood Science Center, Royal Institute of Technology, KTH, SE-10044 Stockholm, Sweden

[‡]Molecular Materials, Department of Applied Physics, Helsinki University of Technology/Aalto University, FIN-00076 Finland

[§]Department of Materials Science, Royal Institute of Technology, SE 10044 Stockholm, Sweden

ABSTRACT: Nacre-mimicking hybrids of high inorganic content (>50 wt %) tend to show low strain-to-failure. Therefore, we prepared clay nanopaper hybrid composite montmorillonite platelets in a continuous matrix of nanofibrillated cellulose (NFC) with the aim of harnessing the intrinsic toughness of fibrillar networks. Hydrocolloid mixtures were used in a filtration approach akin to paper processing. The resulting multilayered structure of the nanopaper was studied by FE-SEM, FTIR, and XRD. Uniaxial stress−strain curves measured in tension and thermal analysis were carried out by DMTA and TGA. In addition, fire retardance and oxygen permeability characteristics were measured. The continuous NFC matrix is a new concept and provides unusual ductility to the nanocomposite, allowing inorganic contents as high as 90% by weight. Clay nanopaper extends the property range of cellulose nanopaper and is of interest in self-extinguishing composites and in oxygen barrier layers.

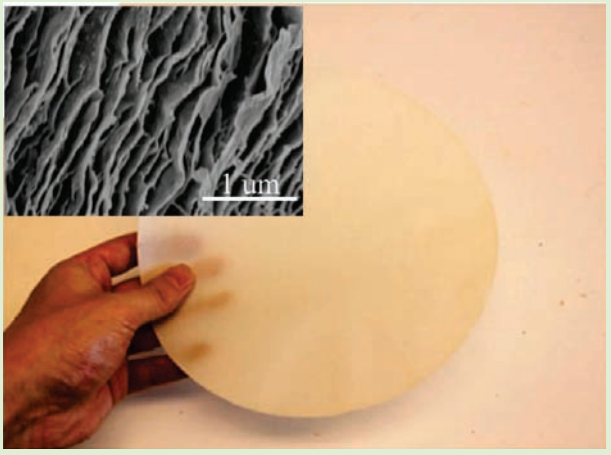

INTRODUCTION

Polymeric-inorganic hybrid composites are widely used industrially. One example from the automotive industry is melt-processable polymer−clay nanocomposites developed by researchers at Toyota.[1] These nanocomposites show improved mechanical, thermal and gas barrier properties at low clay contents,[2] typically below 10 wt %. Reasons include nanoscale dimension of silicate platelets, large aspect ratio, high intrinsic platelet modulus and strength, as well as low thermal expansion. Furthermore, the structure and molecular mobility of the polymer matrix itself may be strongly influenced by the nanoscale silicates.[3] By epoxy impregnation of porous clay films[4] or casting from a hydrocolloidal dispersion of a water-soluble polymer and montmorillonite (MTM),[5] composite clay contents exceeding 50 wt % can be obtained. However, already with clay contents exceeding 5 wt %, nanocomposites in bulk form tend to show lowered strength, as exemplified by PA 6-MTM.[2] This is due to the formation of larger scale MTM agglomerates functioning as defects in a brittle material.

In nature, nanostructured inorganic−organic hybrid composites form tissues of high mechanical functionality[6] such as bone, antler, enamel, dentin, nacre, sea shells, and egg shells. Nacre in particular has attracted attention because it combines high inorganic content with a favorable combination of modulus, strength, and toughness.[7] The structure is often termed a *brick and mortar structure*, consisting of thi3n protein adhesive layers bonding microscale calcium carbonate platelets.[8] Nacre has been mimicked in film structures, a maximum of a few μm in thickness, where inorganic platelets are embedded in a polymer matrix. The following studies use preparation techniques providing nanostructural control but are cumbersome and time-consuming. MTM-polyelectrolyte films of up to 5 μm thickness were prepared using layer-by-layer (LbL) deposition techniques.[9,10] In this type of thin films, greatly improved modulus and strength was later reported for MTM-PVA composites,[11] although strain-to-failure was very low. Repeated spin coating of chitosan and monolayer transfer of Al_2O_3 platelets were used to generate ordered thin hybrid composite materials,[12] which combined 10 GPa modulus with high strength and toughness. Al_2O_3-PMMA hybrids with high crack-growth toughness were prepared by ice-templating, freeze-drying, and sintering of ceramic mixtures, followed by monomer impregnation and polymerization.[13] Still, it remains a challenge to prepare large samples of thick (>50 μm) polymer nanocomposites with a high inorganic content (>50 wt %) and yet high toughness in tension. Such materials would be interesting not only in high-technology applications and coatings, but also in larger composite structures with mechanical function. It is therefore of interest to consider more facile preparation routes.

Recently, a large-scale self-assembly method was used to prepare nacre-mimicking structures based on water-soluble

Received: October 29, 2010
Revised: January 7, 2011
Published: February 03, 2011

polymers and MTM.[14,15] A hydrocolloidal dispersion of silicate platelets is mixed with a water-soluble polymer solution. The platelets adsorb the polymer so that the platelets are coated with the polymer, and excess polymer is removed. The colloidal dispersion of polymer-coated platelets is vacuum-filtrated in a paper-like process and the wet cake is dried. Films of thicknesses in the 5 − 250 μm range are conveniently prepared. With a dried PVA matrix, the stiffest and strongest composition showed a modulus of 45 GPa, a strength of 250 MPa and a strain-to-failure of 0.9%. Thus, although the materials are stiff and strong, and the paper processing route is facile, a remaining challenge is to design materials with increased strain-to-failure. This could increase toughness defined as work-to-fracture, which is proportional to the area under the stress−strain curve. The nacre-mimicking materials rely on matrix failure processes[13] and platelet pull-out[12] as major mechanisms increasing strain-to-failure, so it is of obvious interest to investigate other possibilities.

Among biological composites, compact bone and antler are relevant sources of inspiration for tough organic−inorganic hybrid composites. In principle, the structure of bone (and antler bone) is that of a collagen fibril framework as a templating matrix phase with very small nanoscale inorganic hydroxylapatite platelets as strength and stiffness enhancing reinforcements.[16] The role of the hydrated collagen fibril network for bone toughness has been analyzed.[17] During tensile loading postyield strain and toughness have been directly related to collagen fibril stretching.[18]

In a composite materials context, bone and antler may be viewed as a fibrillar collagen matrix with inorganic platelets dispersed as reinforcement. In previous studies, we disintegrated cellulose nanofibers from wood[19] and prepared cellulose nanopaper of unusual toughness.[20] In the present study, cellulose nanofibers are used as a continuous fibril matrix in organic−inorganic hybrids based on ordered MTM platelets. The use of nanofibers as a continuous matrix represents a new bioinspired concept for man-made nanocomposites. A fibrous matrix may provide new toughening mechanisms inspired by the mechanical function of collagen in bone and antler. In addition, MTM platelets can impart additional functions such as fire retardance[14,15,21] and oxygen barrier properties[5] to hybrid composites. The objectives are to investigate processing feasibility and discuss structure−property relationships for nanoplatelet/nanofiber compositions with large weight fraction of MTM. Paper processing takes place at room temperature, is performed with water as a medium and can easily be scaled to industrial nanocomposites production.

EXPERIMENTAL SECTION

Materials. The clay was a sodium montmorillonite (Cloisite Na^+, Southern Clay Products) with a cation-exchange capacity (CEC) of 92 mequiv/100 g. The average size of the platelets is 110 nm, as described by the manufacturer. A 1.0 wt % clay dispersion, used in the experiments, was prepared by dispersing 10 g of clay in 1 L of deionized water under vigorous stirring before use.

Nanofibrillated cellulose (NFC) dispersion was prepared according to the work by Henriksson et al.[19] Degree of polymerization (DP) was estimated to 480 from the average intrinsic viscosity after homogenization. NFC dispersion with 1.63 wt % solid content was obtained and stored at 4 °C.

Preparation of Clay Nanopaper. NFC/clay nanopapers with 11, 20, 33, and 50 wt % NFC were prepared as follows. A 1.63 wt % NFC dispersion containing 1.5, 1.0, 0.5, and 0.5 g of NFC was slowly added to a 1.0 wt % clay dispersion containing 1.5, 2, 2, and 4 g of clay to obtain mixture dispersions with weight ratios of NFC to clay of 1:1, 1:2, 1:4, and 1:8, coded as 50N/50M, 33N/67M, 20N/80M, and 11N/89M, respectively. The mixed dispersion was stirred for 24 h and then was further dispersed for 30 min by ultrasonic equipment. Then the mixtures were vacuum-filtrated by Rapid Köthen using filter membrane, 0.65 μm DVPP, Millipore, U.S.A. (polyvinylidene fluoride microfiltration membranes, hydrophilic Durapore, 0.65 μm average pore diameter, 125 μm thickness, catalogue #DVPP 047 00). The filtration time ranges from 30 to 90 min, depending on the thickness of the final nanopaper and the concentration of clay. After filtration, the wet films were carefully peeled off from the filtration membrane and stacked between metal grids, and then everything was placed between two filter papers. Finally, clay nanopapers with a thickness in the range of 60−80 μm were obtained after dried by vacuum at 93 °C for 10−15 min. Figure 1b shows the sketch of preparation process of clay nanopaper.

Characterization of Clay Nanopaper. Wide-angle XRD patterns of the obtained films were recorded by a Siemens D5000 X-ray diffractometer at room temperature. The CuKα radiation source was operated at 40 kV and 40 mA. Patterns were recorded by monitoring diffractions from 1.5 to 10°. The scan speed was 2°/min. Two-dimensional X-ray diffraction (XRD) photographs were taken by an imaging plate (IP) having a camera length of 38.3 mm. The Cu Kα radiation, generated with a Rigaku RINT-2000 at 40 kV, 35 mA, was irradiated on the specimen perpendicular or parallel to the film surface.

The density was determined for dry clay nanopaper. The volume of sample was measured manually with a caliper and thickness meter. The porosity was obtained from $(1 - [\rho^*/\rho_t]) \times 100\%$, where ρ^* is the nanopaper density and ρ_t is the theoretical density of nanopaper. ρ_t was obtained from the densities of the constituents (ρ_i, $i = 1, 2, ..., n$) and their weight fraction (W_i, $i = 1, 2, ..., n$):

$$\rho_t = \frac{1}{\sum_{i=1}^{n} W_i/\rho_i} \quad (1)$$

Fourier transform infrared (FTIR) spectra (transmission) were measured on a Perkin-Elmer FTIR spectrophotometer 2000 in the range of 4000−400 cm^{-1} at a resolution of 4 cm^{-1}.

The morphology was examined with a JEOL JSM-820 scanning electron microscope. The samples were held in liquid N_2 and a brittle fracture was performed. A few nm thick layer of gold was sputtered onto the surface of cross sections prior to imaging.

The tensile tests of the films were performed with a Universal Materials Testing Machine from Instron, U.S.A., equipped with a 100 N load cell. Specimens of 40 mm length and 60−80 μm thickness and 5 mm width were tested with strain rate of 4 mm/min. The relative humidity was kept at 50% and the temperature at 23 °C. The specimens were conditioned for at least 48 h in this environment prior to testing. The displacement was measured by Digital Speckle Photography (DSP). A pattern was prepared for the DSP by applying printer toner to the sample surface. During tensile test images of the whole specimen was taken. The frame rate was set to 5 fps. The results for each material are based on at least 6 specimens, if nothing else is mentioned.

The dynamic mechanical analysis (DMA) of the films was measured with TA Instruments Q800 in tensile mode. The distance between the grips is 10 mm and the heating rate was 3 °C/min. The specimens, with thickness varying between 60 and 80 μm and a width of 5 mm, were dried in a vacuum oven at 50 °C prior to the analysis.

The thermogravimetric analysis (TGA) was conducted on a Perkin-Elmer TGA 7-thermal analyzer from 25 to 800 °C, with a heating rate of 10 °C/min under oxygen with a flow rate of 50 mL/min.

Self-extinguishing flammability test: A specimen of 6×1 cm was used. The specimen was mounted in a holder at a 45° angle and exposed to flame for 1 s. After ignition, the flame was removed.

The permeability of the material to oxygen at 23 °C was determined using a Mocon OX-TRAN TWIN equipped with a coulometric oxygen

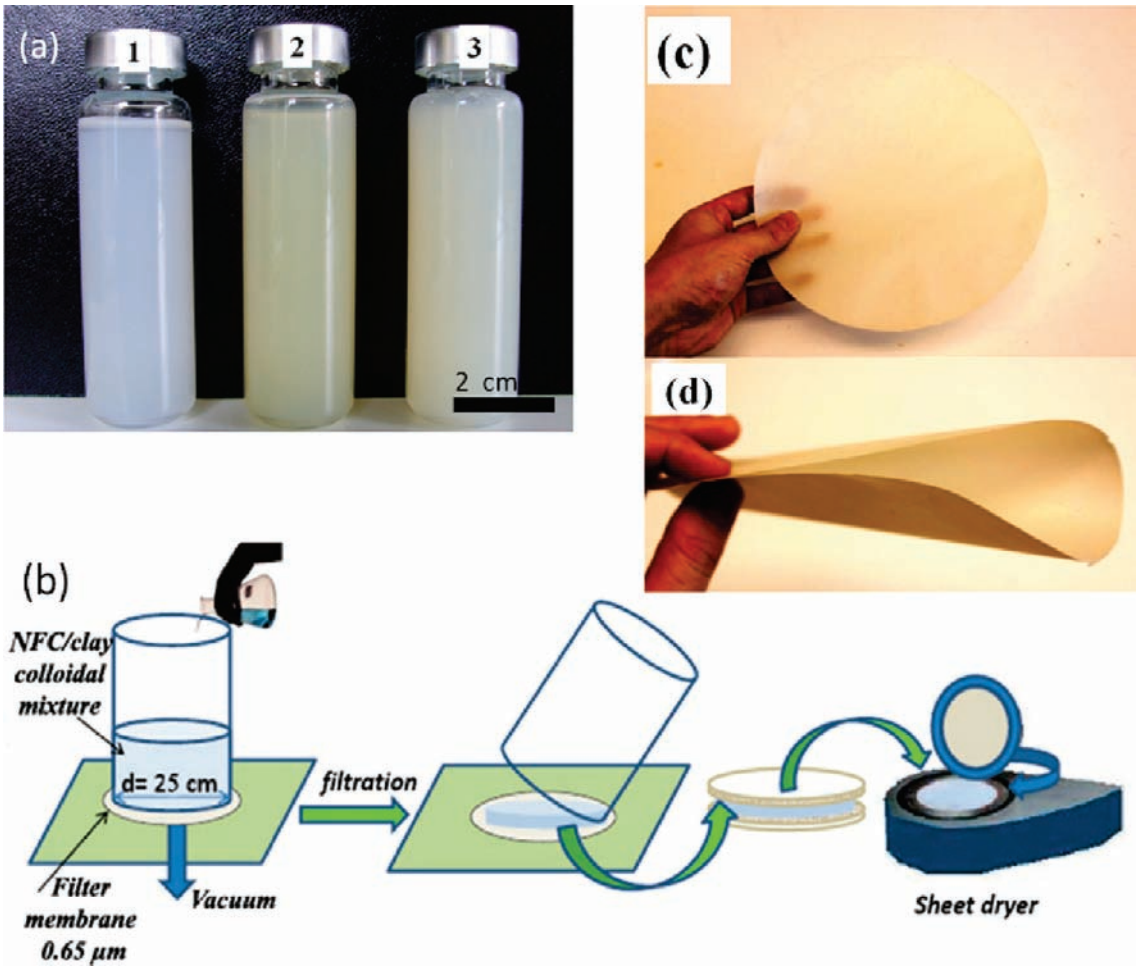

Figure 1. Preparation of clay nanopaper. (a) Photograph of 0.62 wt % NFC dispersion (a1), 0.62 wt % MTM dispersion (a2), and NFC/MTM (0.62 wt %/0.62 wt %) codispersion (a3) in aqueous solution after 10 h. (b) Sketch of the preparation process of clay nanopaper. (c) Free standing 50 N/50 M clay nanopaper showing a large-area and translucent sample. (d) Illustration of flexibility in free-standing 11 N/89 M clay nanopaper.

sensor. Degassed film samples with thickness of 60 ± 20 μm were mounted in an isolated diffusion cell and were subsequently surrounded by flowing nitrogen gas to remove sorbed oxygen from the samples. The sample had a circular exposure area of 100 × 10^{-4} m^2 achieved by covering a part of the film with a tight aluminum foil that has an adhesive on its surface. One side of the sample was initially exposed to flowing oxygen containing 1% hydrogen at atmospheric pressure. The oxygen pressure was zero on the other side. The flow rate (Q) through the sample was measured and, from the steady-state flow rate (Q_∞), the oxygen transmission rate (OTR) was calculated.

RESULTS AND DISCUSSION

Dispersion State of NFC and Clay in Aqueous Solution. The cellulose I/layered silicate nanopaper (clay nanopaper) composite is based on two components: a montmorillonite layered silicate (MTM) and wood-based cellulose nanofibers in the form of nanofibrillated cellulose (NFC).[19,22−24] The NFC nanofibers are prepared by enzymatic wood fiber pretreatment followed by mechanical disintegration. The lateral dimensions of NFC are 10−30 nm from an AFM micrograph of the nanopaper surface.[19] The nanofiber length exceeds 1 μm so that the aspect ratio (length/diameter) is typically above 100. A nanofibrous paper network forms during casting as water evaporates from the supension.[20]

The preparation strategy is to first prepare a NFC hydrocolloid and combine it with a colloidal dispersion containing discrete nanoplatelets exfoliated from a layered montmorillonite silicate (MTM). Initially, NFC was well dispersed in water, see Figure 1a1. The NFC surface has a slight negative charge, repelling individual nanofibers from each other. Figure 1a2 illustrates that the hydrocolloid dispersion of MTM is very stable, with virtually no precipitation of MTM clay aggregates in the observed time frame. The major platelet proportion is therefore suspended discretely in an exfoliated state,[11] although small platelet agglomerates may also be present. The stability of the dispersions illustrated in (a1) and (a2) is a helpful condition for the next blending step. Figure 1a3 illustrates that the blended dispersion of NFC and MTM is very stable, even after 10 h. The negative surface charge on both NFC and MTM helps toward mutual repellence of the two components in aqueous dispersion.

Structure of Clay Nanopaper. The preparation of the clay nanopaper is outlined in Figure 1b. The NFC-clay hydrocolloid mixture was first vacuum filtrated, followed by drying of the wet nanofiber/silicate cake in a Rapid Köthen apparatus.[25] The complete fabrication time to obtain a 250 mm diameter film of 60−80 μm thickness ranges from 30 to 90 min, depending on the final thickness and MTM content. Figure 1c shows the free-standing clay nanopaper with large-area and acceptable transparency. The

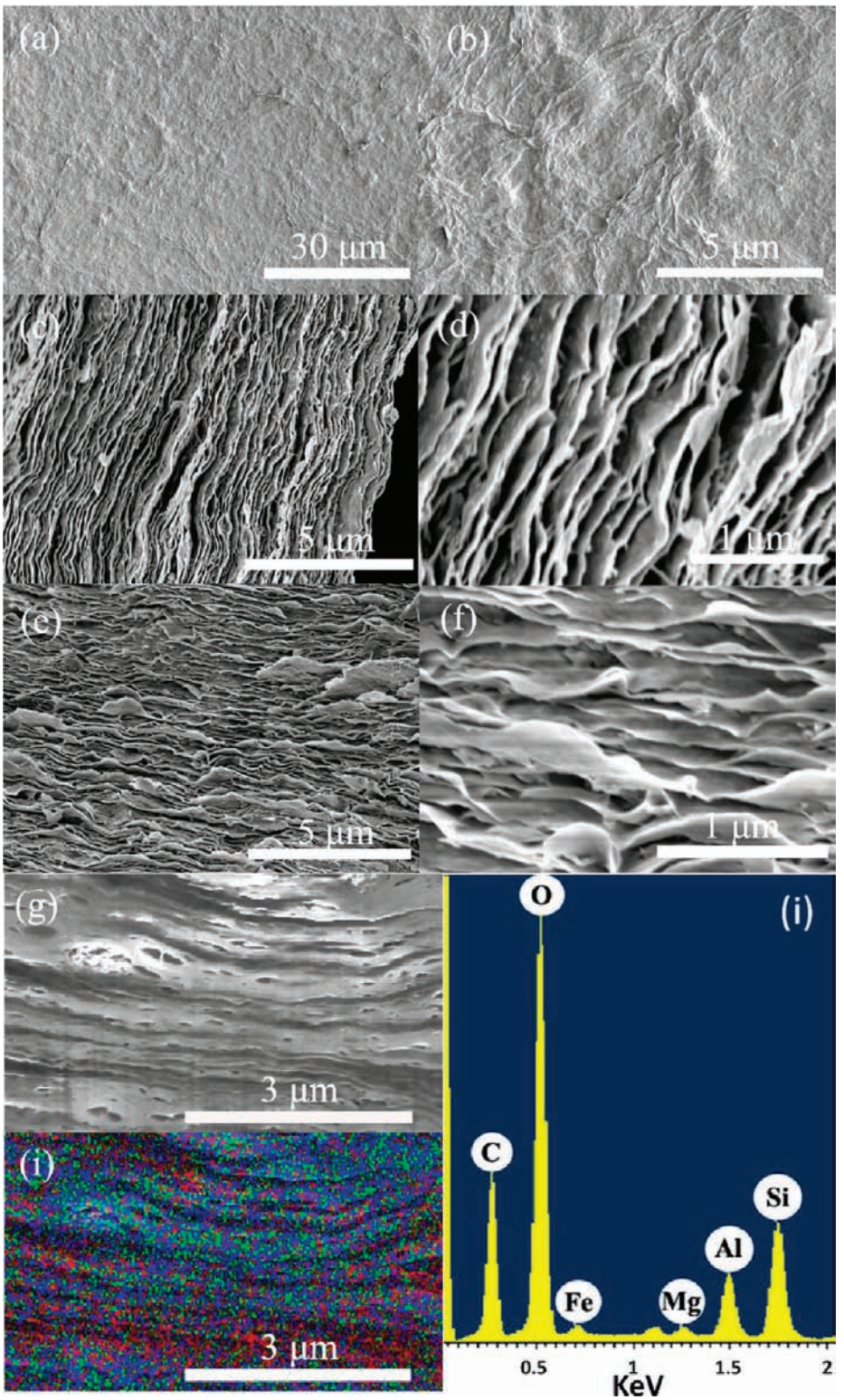

Figure 2. FE-SEM images of surfaces of 50N/50 M (a, b). Images of the cross-section of cryo-fractured surfaces of 50N/50 M (c, d) and 20N/80 M (e, f). FE-SEM images (g), EDX image (h) (red-carbon, green-aluminum and blue-silicon, the spatial distribution is about 8 μm × 8 μm) and EDX spectrum (i) of the ion-milled cross-section of 50N/50M.

impressive flexibility of a clay nanopaper with 89 wt % clay is depicted in Figure 1d. Consequently, this is a quick, large-scale procedure, considering the nanostructured characteristics of the material obtained.

The surface of nanopaper is microscopically flat (Figure 2a) although surface inhomogeneities were observed at the 1 μm scale (Figure 2b). SEM images of cross sections of cryo-fractured surfaces of 50 N/50 M (Figure 2c,d) and 20 N/80 M (Figure 2e,f)

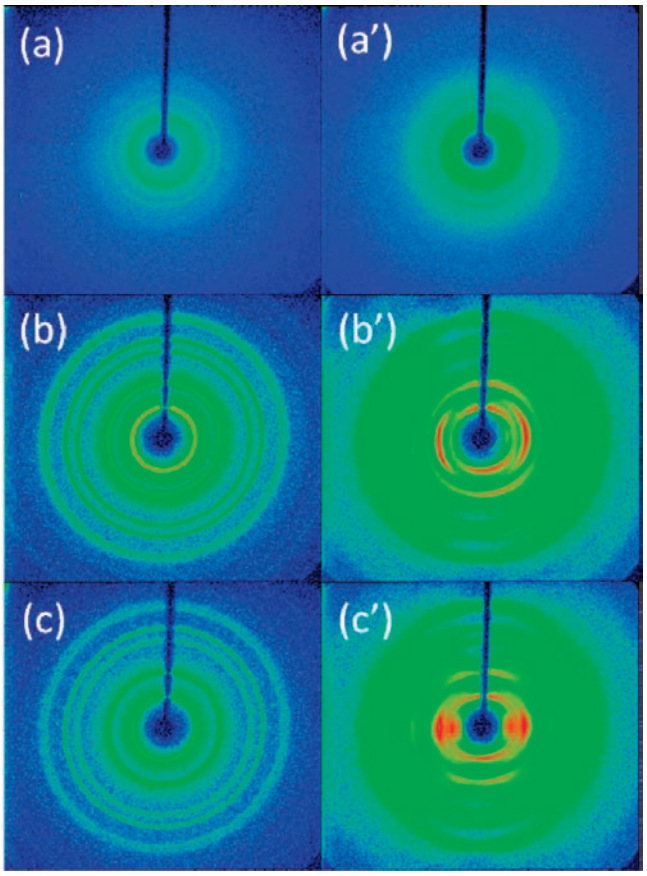

Figure 3. Two-dimensional XRD data on NFC film (a, a′), MTM film (b, b′), and 50 N/50 M clay nanopaper film (c, c′) perpendicular (a−c) and parallel (a′−c′) to the film surface plane.

are also presented. A layered structure reminiscent of nacre is apparent.[26,27] The layered structure appears regular, and the layer thickness is fairly uniform with a scale below 100 nm. The sheet-like structures are parallel to the film surface. The layers have a slightly wavy appearance and are interpenetrating into neighboring layers. This phenomenon was also observed in biomimetic organic−inorganic composites made from PVA/clay by LbL or MTM/polymer self-assembly.[9,11,14,15] A more flat ion-milled surface of 50 N/50 M was also observed (Figure 2g). Therein, submicrometer-scale pores can be identified. The porosity is estimated from the clay nanopaper density by assuming constituent densities of 1500 kg/m^3 for NFC and 2860 kg/m^3 for clay. The density of 50 N/50 M is 1483 kg/m^3. Hence, the porosity of 50 N/50 M is about 32% based on eq 1, which is similar to typical values for pure NFC films.[20] From the energy-dispersive X-ray analysis (EDX) element maps (Figure 2h,i), the clay components (green-aluminum, blue-silicon) show a fairly homogeneous distribution, whereas the NFC distribution (red-carbon) gives a more inhomogeneous impression. The clay nanopaper cross-section surface is probably not perfectly flat after ion-beam milling.

The nanoscale layered structure observed is somewhat unexpected in a paper-like preparation process suitable for large-scale manufacturing. For LbL self-assembly,[9] films with multilayers are formed through sophisticated but tedious alternating sequential deposition of negatively and positively charged layers. The primary driving force for multilayer formation is electrostatic or hydrogen-bonding interaction. For the present batch-processed clay nanopaper, one may speculate that established mechanisms for flocculation during papermaking may to some extent explain the multilayered structure.[20] Significant flocculation tends to occur when fiber concentration increases in the region closest to the membrane filter.

Orientation Distribution of NFC and MTM. The orientation distribution of platelets in a pure MTM film,[28] fibrils in cellulose nanopaper,[22] and the present clay nanopaper was studied by two-dimensional X-ray diffraction (XRD). Figure 3 presents XRD data perpendicular and parallel to the film surfaces. Diffraction arcs are characteristic of preferred orientation and diffraction rings correspond to random orientation. In Figure 3a, the orientation of cellulose nanofibers in the surface plane appears as completely random. In the perpendicular direction, there is a weak meridional arc observed, see Figure 3a′. Cellulose nanofibers therefore show order in this plane, although weaker in this sample than in previously reported nanopaper data.[20] We expect cellulose nanofibers to be predominantly in-plane rather than in-space oriented because they are deposited flatly in swirled conformations on the membrane during vacuum filtration.[20] The data for MTM platelet films show preferred orientation parallel to the surface plane, see Figure 3b,b′. For the mixed 50 N/50 M clay nanopaper films, the orientation of MTM and NFC in the plane parallel to the surface is again completely random, whereas it is ordered in the cross-sectional plane, see Figure 3c,c′. The data are consistent with the electron micrographs in Figure 2.

Interaction between NFC and MTM. FTIR spectroscopy was used to characterize the molecular interaction between NFC and MTM. Figure 4a shows the IR spectra of MTM, NFC, and clay nanopaper films with different MTM clay contents. The frequency of vibrational bands at 3610 cm^{-1} corresponds to hydrogen bonding in MTM and the frequency of vibrational bands at 3330 cm^{-1} corresponds to hydrogen-bonding in cellulose I (NFC).[29] The peak intensity is strong for cellulose I hydrogen bonding in pure NFC, due to the high density of hydroxyl groups. However, for 50 N/50 M and 20 N/80 M, the intensity of hydrogen bonding in NFC is weakened and shifted toward higher frequency value (from 3330 to 3386 cm^{-1}). This is partly due to decreased NFC concentration, but also indicates that interfibril hydrogen bonding in NFC is influenced by the presence of MTM clay platelets. It suggests that NFC nanofibers are adsorbed to the silicate platelet surfaces, so that the extent of interfibril hydrogen bonding is reduced. It confirms the impression from SEM micrographs that NFC is well dispersed in the nanocomposites. As Figure 4b shows, we also observe a very weak peak at 840 cm^{-1} corresponding to the vibration of Al−O−C, which may indicate the formation of Al−NFC bonds via the hydroxyl group of the NFC interacting with the Al on the clay platelet surface. Although there is a peak, we cannot interpret it as a strong interaction. This is also supported by the lack of intercalation discussed in the coming section, as well as in the mechanical property results.

XRD data from clay nanopaper with MTM contents of 50, 67, 80, and 89% by weight showed no change in MTM basal-space reflection peaks with a *d*-spacing value of around 1.2 nm. Thus, there is no sign of intercalation of cellulose nanofibers in the MTM galleries. Note that we did not expect a quantitative intercalation and separation of the MTM platelets due to the intrinsic thickness of the NFC nanofibers as compared to standard polymers used earlier for nacre-mimetic materials.

Colloidal fibers cannot allow a full intercalation for ultrathin clay platelets in a bulk composite at these weight ratios.

Sketch of Clay Nanopaper. Based on the SEM micrographs, XRD data, FTIR data, and arguments presented, a schematic sketch of the proposed nanopaper structure is presented in Figure 5. Nacre-like structures from LbL self-assembly show alternating multilayer structure, in which one layer-type is clay and the other layer-type is a polymer.[9] Recently, a paper-like preparation procedure was used to produce a nacre-like multilayer structure consisting of MTM platelets in a polymer matrix.[14,15] Here, one difference is that the polymer matrix is replaced with an NFC cellulose nanofiber matrix. In vertical surface direction, the clay nanopaper has a lamellar structure, see Figure 5. However, the NFC nanofibers (green line) entangle and form a fibrous network matrix surrounding the platelets as the total amount of NFC is insufficient to completely intercalate all MTM galleries.

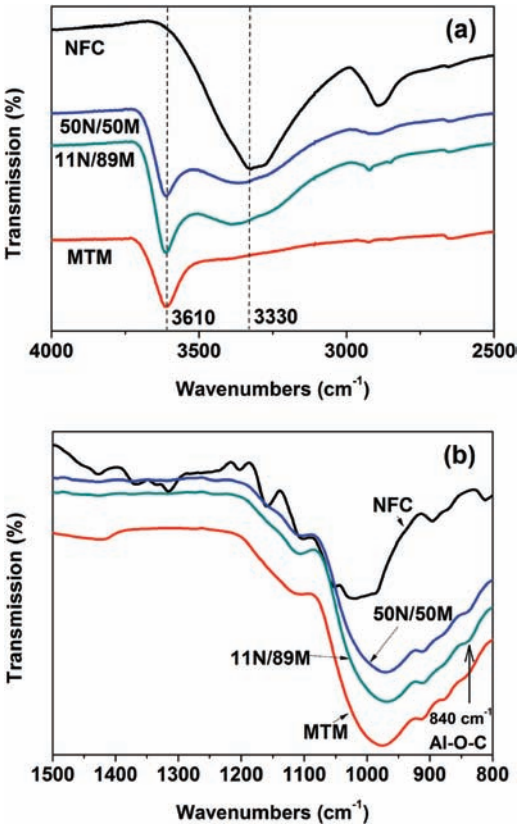

Figure 4. FTIR spectra (ranging from 4000 to 2500 cm^{-1} (A) and from 1500 to 800 cm^{-1} (B)) of NFC, MTM, and clay nanopaper with a different content of MTM (50 and 89% by weight).

Mechanical Properties of Clay Nanopaper. Neat MTM films are very brittle, which impedes many potential applications. Also, layered silicate nanocomposites become extremely brittle as the MTM content is increased above a few percent by weight.[4,30,31] In contrast, clay nanopaper may have potential for a more ductile behavior due to the NFC. As we reported before, NFC itself is quite strong with about 200 MPa of tensile strength and 10 GPa of modulus.[19,20] Thus, we expected the NFC fibrils to give a robust matrix material in which we could harness the intrinsic toughening of the fibrillar material for the hybrid paper. In Figure 6a, stress−strain curves are displayed for clay nanopaper with different content of MTM. Strain-to-failures in the 2−3% range and the nonlinear curve shape demonstrate ductility despite the high inorganic content. The best combination of properties is obtained with higher NFC content, as shown in Figure 6b. The molecular interaction between NFC and layered MTM silicate platelets is insufficient for effective load transfer from the continuous NFC nanofiber matrix to the MTM platelets.

The 50 N/50 M nanopaper shows interesting characteristics. At 50 wt % MTM content, the ultimate strength and Young's modulus are 124 MPa and 8.7 GPa, respectively. The strength is similar to that of mineralized tissues in nature (100−150 MPa), such as nacre,[32] dentin,[33] and bone,[34] as well as synthetically prepared materials, such as some clay/polyelectrolytes[9] and clay/polyvinyl alcohol[11] multilayer nanocomposites prepared by layer-by-layer self-assembly. The mechanical properties are somewhat lower than for the best self-assembled MTM/polymer composites.[14,15] The 11 N/89 M nanopaper is also interesting and shows 2% strain-to-failure and 30 MPa tensile strength despite its high inorganic content of almost 90%. This clay nanopaper is also remarkably flexible in bending as illustrated in Figure 1d.

Structural characteristics of clay nanopaper explain the mechanical properties. First, both MTM platelets and NFC nanofibers are oriented in the plane, which provides anisotropy and favorable potential for in-plane mechanical behavior. Because NFC forms a continuous nanofiber network matrix, favorable failure characteristics are introduced in terms of more ductile behavior. Recent multilayered nanocomposites hybrids based on MTM and polymer matrices show superior Young's modulus and

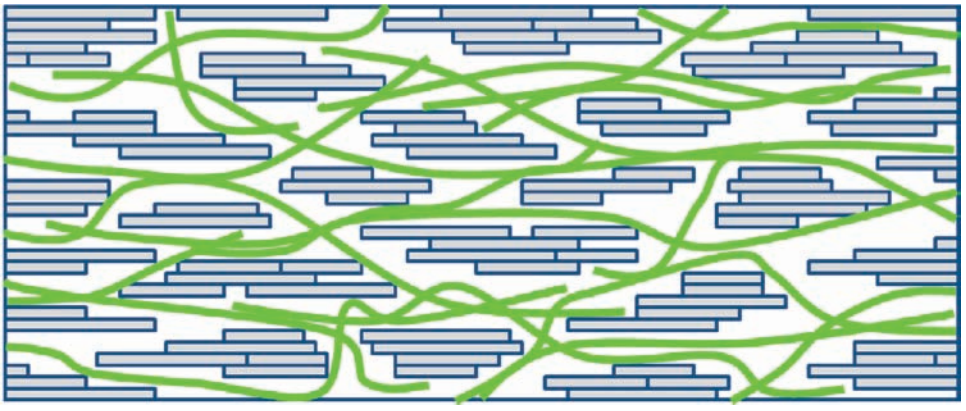

Figure 5. Schematic representation of the structure of the nanopaper cross-sectional surface plane.

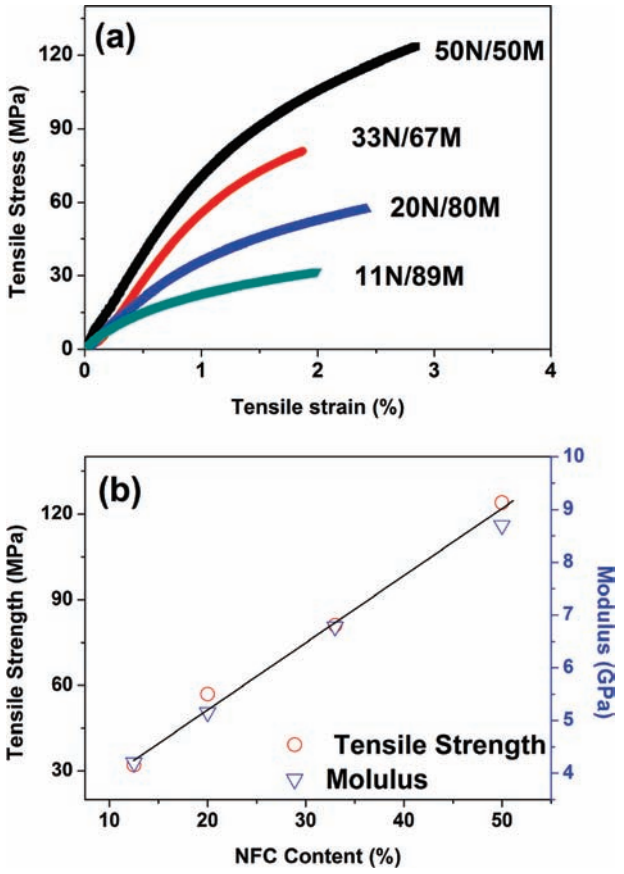

Figure 6. Stress−strain curves in tension for clay nanopaper with different content of MTM (a) and linear correlation of strength and modulus of nanopaper with NFC content, respectively (b).

ultimate strength compared to the present materials.[11,14] The main reason is stronger interfacial matrix−MTM interaction and quantitative exfoliation of the clay platelets. In more detail, the strength and modulus show positive linear correlations with the NFC content (Figure 6b), indicating that the continuous NFC network is the major load-carrying phase. The reason for the absence of load transfer onto the clay nanoplatelets can be identified in the insufficient NFC−MTM interfacial adhesion. However, the NFC nanofibers represent a conceptually new and attractive matrix with potential for fast processing of large-area nanocomposites with very high inorganic content, high porosity, and considerable ductility.

Thermal Stability, Flame Retardance, and Barrier Properties of Clay Nanopaper. The DMA data (Figure 7) for the 50 N/50 M clay/NFC hybrid nanopaper shows a storage modulus of 11.0 GPa at room temperature. Even at 200 °C, the storage modulus is still as high as 8.7 GPa. This is a much better thermal stability in terms of modulus than what can typically be obtained with polymers or nanocomposites. Again, the reason is the structural organization and inherent characteristics of MTM and mechanically robust NFC cellulose nanofibers, combined with intimate mixing. The reason for the increasing mechanical damping with temperature is not clear but may involve frictional effects at nanoscale interfibril interfaces.

Aside mechanical performance, inorganic materials impart further functionality and allow multifunctional inorganic−organic hybrid composites. In particular, the area of materials reinforced with a high content of inorganics is a rather unexplored terrain. Fire retardance

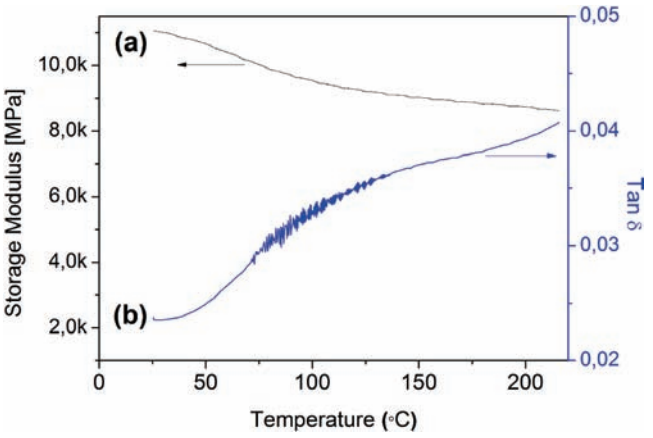

Figure 7. Storage modulus E' (a) and mechanical damping tan δ (b) as a function of temperature for 50 N/50 M clay/NFC hybrid nanopaper (b).

is an important measure of performance for fiber composites, including biocomposites. In aircraft, train, and building interiors, fire retardant composite structures are highly desirable. We therefore measured the self-extinguishing characteristics of clay nanopaper using a 45° flammability test. In Figure 8a,b, photographs of clay nanopaper with 80 and 50 wt % of MTM are presented before and after the test. Pure NFC has high flammability and burns quickly and completely. However, the photographs illustrate that clay nanopaper is immediately self-extinguishing upon removal of the flame, even at 50 wt % MTM content. Similar observations were reported for self-assembled MTM−polymer nanocomposites.[14,15] Even if the present clay nanopaper has a dimension as large as 100 × 100 mm (Figure 8c), it maintains shape and integrity after burning in cone calorimeter.

TG-DTA results of clay nanopaper with different content of MTM are presented in Figure 8d,e. For NFC, there are two degradation stages, which can be divided into thermal cracking at 250−350 °C and carbonization at 400−500 °C. As expected, the decomposition rate for two stages increased with increasing NFC cellulose content, and high inorganic content is obviously advantageous. Despite this "ceramic" composition, even the clay nanopaper with 89% silicate resembles regular nanopaper in terms of flexibility and mechanical robustness during handling.

The TGA curves in Figure 8d,e demonstrate that the degradation rate of clay nanopaper is much slower compared with that of NFC cellulose nanopaper. The heat release is so slow that combustion of NFC cannot be supported. Silicate platelets are inorganic but also hinder oxygen transport and diffusion of decomposition products,[35,36] hence, improving the resistance of the material against burning.

Because MTM is interesting as a barrier against gas diffusion,[4] oxygen permeability was measured on clay nanopaper under dry and 50% relative humidity (RH) conditions, as shown in Table 1. The oxygen transmission rate (OTR) of dry 50 N/50 M clay nanopaper was less than 0.001 cm^3 mm m^{-2} day^{-1} atm^{-1}. This is better than for synthetic polymer films such as ethylene-vinyl alcohol copolymer, polyvinyl chloride, and polyvinyl alcohol widely used as oxygen barriers.[37] The layered structure and the structural ordering of MTM increases the diffusion length for oxygen, according to the tortuous-path model.[38] Additionally, NFC has inherently high degree of molecular ordering and also shows low oxygen permeability.[39] The OTR of 50 N/50 M clay

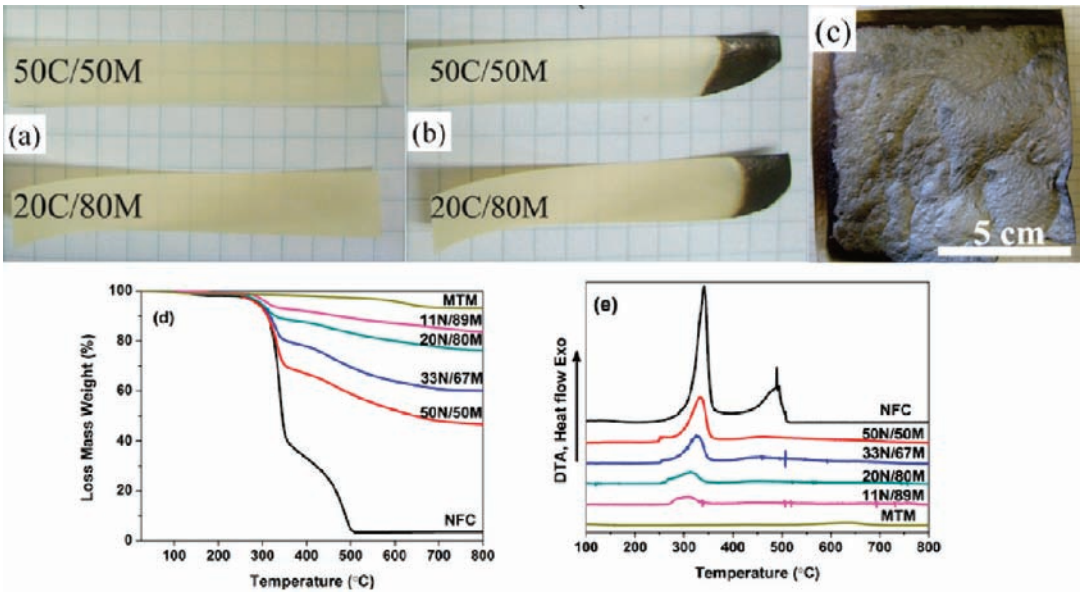

Figure 8. Photographs of 50 N/50 M and 20 N/80 M clay nanopaper before burning (a) and after burning (b) in air. The sample size is 60 mm × 10 mm × ~70 μm. Photographs of the surface of large sample (100 × 100 mm) of 50 N/50 M after burning by cone calorimeter (c). Data from TGA (d) and DTA (e) experiments in O_2 environment on clay nanopaper of different MTM silicate content (50, 67, 80, and 89 wt %).

Table 1. OTR (cm^3 mm m^{-2} day^{-1} atm^{-1}) of NFC and 50 N/50 M Clay Nanopaper under 0, 50, and 95% Relative Humidity (RH) and 100% Oxygen Conditions

samples	0% RH	50% RH	95% RH
NFC	[a]	0.048	17.8
50 N/50 M	[a]	0.045	3.5

[a] OTR at 0% RH 100% O_2 for these materials was below detection limit.

nanopaper at 50% RH increased to 0.045 cm^3 mm m^{-2} day^{-1} atm^{-1}. Both NFC and stacked silicate layers are hydrophilic and are swollen by water. However, this result is still better than for some biopolymers, for example, polylactic acid (PLA). When the RH was increased to 95%, the OTR of NFC increased 375×, nearly exponentially. Water molecules above a certain water activity level can disrupt hydrogen bonding and van der Waals interactions, creating additional sites for the permeation of oxygen and an increased mobility of oxygen molecules within the NFC network. However, the OTR of NFC−MTM hybrid nanopaper at 95% RH is much lower than that of pure NFC, demonstrating a clear benefit originating from the MTM. The layered structure of the hybrid nanopaper and the in-plane orientation of MTM increase the diffusion path length of small gas molecules. Still, the hydrophilicity of nanopaper is a problem that needs to be resolved.

CONCLUSIONS

A water-based paper-making procedure has been used to prepare large, flat clay nanopaper hybrid composites with montmorillonite platelets as the inorganic phase. A cellulose nanofiber network forms the continuous matrix phase with random-in-the-plane fibril orientation distribution. This concept has similarities with the collagen matrix in biological composites such as bone and antler. Furthermore, the inorganic platelets were highly organized in the plane parallel to the nanopaper surface, and the preparation procedure is much simpler than classical layer-by-layer deposition techniques. The present multilayer structure showed homogeneous phase mixing at the 100 nm scale. An inorganic content as high as 89% by weight was reached with a maintained and astonishing mechanical robustness. This clay nanopaper composition has a strain-to-failure as high as 2% due to the load-carrying function of the continuous cellulose nanofiber matrix. At 50% by weight of montmorillonite, the tensile strength was 124 MPa and the modulus 8.7 GPa, which we can imagine to be much improved by better NFC−MTM interaction. The clay nanopaper showed self-extinguishing characteristics when subjected to open flames and also much delayed thermal degradation of cellulose, primarily because of the favorable gas barrier properties of ordered clay platelets. Although the oxygen barrier properties of pure cellulose nanopaper are exceptionally good in the dry state, the addition of montmorillonite improves barrier properties considerably at higher relative humidity. The data suggest that clay nanopaper is of great interest for application in self-extinguishing composites and for further development into barrier layers in packaging applications.

AUTHOR INFORMATION

Corresponding Author

*Tel.: +46-8-7908118. Fax: +46-8-7906166. E-mail: blund@kth.se (L.A.B.); andong@kth.se (A.D.L.).

ACKNOWLEDGMENT

BiMaC Innovation is gratefully acknowledged for financial support of A.L.

REFERENCES

(1) Usuki, A.; Kojima, Y.; Kawasumi, M.; Okada, A.; Fukushima, Y.; Kurauchi, T.; Kamigaiton, O. *J. Mater. Res.* **1993**, *8*, 1179–1184.

(2) Okada, A.; Usuki, A. *Macromol. Mater. Eng.* **2006**, *291*, 1449–1476.

(3) Szazdi, L.; Pozsgay, A.; Pukanszky, B. *Eur. Polym. J.* **2007**, *43*, 345–373.
(4) Triantafyllidis, K. S.; LeBaron, P. C.; Park, I.; Pinnavaia, T. J. *Chem. Mater.* **2006**, *18*, 4393–4398.
(5) Strawhecker, K. E.; Manias, E. *Chem. Mater.* **2000**, *12*, 2943–2949.
(6) Meyers, M. A.; Chen, P. Y.; Lin, A. Y. M.; Seki, Y. *Prog. Mater. Sci.* **2008**, *53*, 1–206.
(7) Jackson, A. P.; Vincent, J. F. V.; Turner, R. M. *Proc. R. Soc., B* **1988**, *234*, 415–440.
(8) Espinosa, H. D.; Rim, J. E.; Barthelat, F.; Buehler, M. J. *Prog. Mater. Sci.* **2009**, *54*, 1059–1100.
(9) Tang, Z. Y.; Kotov, N. A.; Magonov, S.; Ozturk, B. *Nat. Mater.* **2003**, *2*, 413–418.
(10) Decher, G. *Science* **1997**, *277*, 1232–1237.
(11) Podsiadlo, P.; Kaushik, A. K.; Arruda, E. M.; Waas, A. M.; Shim, B. S.; Xu, J.; Nandivada, H.; Pumplin, B. G.; Lahann, J.; Ramamoorthy, A.; Kotov, N. A. *Science* **2007**, *318*, 80–83.
(12) Bonderer, L. J.; Studart, A. R.; Gauckler, L. J. *Science* **2008**, *319*, 1069–1073.
(13) Munch, E.; Launey, M. E.; Alsem, D. H.; Saiz, E.; Tomsia, A. P.; Ritchie, R. O. *Science* **2008**, *322*, 1516–1520.
(14) Walther, A.; Bjurhager, I.; Malho, J. M.; Pere, J.; Berglund, L. A.; Ikkala, O. *Nano Lett.* **2010**, *10*, 2742–2748.
(15) Walther, A.; Bjurhager, I.; Malho, J. M.; Berglund, L. A.; Ikkala, O. *Angew. Chem., Int. Ed.* **2010**, *49*, 6448–6453.
(16) Weiner, S.; Traub, W. *FASEB J.* **1992**, *6*, 879–885.
(17) Currey, J. D. *Osteoporosis Int.* **2003**, *14*, 29–36.
(18) Krauss, S.; Fratzl, P.; Seto, J.; Currey, J. D.; Estevez, J. A.; Funari, S. S.; Gupta, H. S. *Bone* **2009**, *44*, 1105–1110.
(19) Henriksson, M.; Henriksson, G.; Berglund, L. A.; Lindström, T. *Eur. Polym. J.* **2007**, *43*, 3434–3441.
(20) Henriksson, M.; Berglund, L. A.; Isaksson, P.; Lindström, T.; Nishino, T. *Biomacromolecules* **2008**, *9*, 1579–1585.
(21) Hussain, M; Varley, R. J.; Mathys, Z.; Cheng, Y. B.; Simon, G. P. *J. Appl. Polym. Sci.* **2004**, *91*, 1233–1253.
(22) Herrick, F. W.; Casebier, R. L.; Hamilton, J. K.; Sandberg, K. R. *J. Appl. Polym. Sci, Appl. Polym. Symp.* **1983**, *37*, 797–813.
(23) Turbak, A. F.; Snyder, F. W.; Sandberg, K. R. *J. Appl. Polym. Sci., Appl. Polym. Symp.* **1983**, *37*, 815–827.
(24) Morseburg, K.; Chinga-Carrasco, G. *Cellulose* **2009**, *16*, 795–806.
(25) Sehaqui, H.; Liu, A. D.; Zhou, Q.; Berglund, L. *Biomacromolecules* **2010**, *11*, 2195–2198.
(26) Sarikaya, M.; Aksay, I. A. Biomimetics: Design and Processing of Materials, American Institute of Physics: New York, 1995.
(27) Aksay, I. A.; Trau, M.; Manne, S.; Honma, I.; Yao, N.; Zhou, L.; Fenter, P.; Eisenberger, P. M.; Gruner, S. M. *Science* **1996**, *273*, 892–898.
(28) Rao, Y. Q.; Blanton, T. N. *Macromolecules* **2008**, *41*, 935–941.
(29) Liang, C. Y.; Marchessault, R. H. *J. Polym. Sci.* **1959**, *37*, 385–395.
(30) Ebina, T.; Mizukami, F. *Adv. Mater.* **2007**, *19*, 2450–2453.
(31) Tetsuka, H.; Ebina, T.; Nanjo, H.; Mizukami, F. *J. Mater. Chem.* **2007**, *17*, 3545–3550.
(32) Wang, R. Z.; Suo, Z.; Evans, A. G.; Yao, N.; Aksay, I. A. *J. Mater. Res.* **2001**, *16*, 2485–2493.
(33) Sano, H.; Ciucchi, B.; Matthews, W. G.; Pashley, D. H. *J. Dent. Res.* **1994**, *73*, 1205–1211.
(34) Landis, W. J.; Librizzi, J. J.; Dunn, M. G.; Silver, F. H. *J. Bone Miner. Res.* **1995**, *10*, 859–867.
(35) Gilman, J. W.; Jackson, C. L.; Morgan, A. B.; Harris, R.; Manias, E.; Giannelis, E. P.; Wuthenow, M.; Hilton, D.; Philips, S. H. *Chem. Mater.* **2000**, *12*, 1866–1873.
(36) Gilman, J. W. *Appl. Clay Sci.* **1999**, *15*, 31–49.
(37) Lange, J.; Wyser, Y. *Packag. Technol. Sci.* **2003**, *16*, 149–158.
(38) Nielsen, L. E. *J. Macromol. Sci.* **1967**, *A1*, 929–942.
(39) Fukuzumi, H; Saito, T.; Iwata, T.; Kumamoto, Y.; Isogai, A. *Biomacromolecules* **2009**, *10*, 162–165.